ACS APPLIED POLYMER MATERIALS

pubs.acs.org/acsapm Article

Promoting Bandlike Transport in Well-Defined and Highly Conducting Polymer Thin Films upon Controlling Dopant Oxidation Levels and Polaron Effects

Jonathan Ogle, Daniel Powell, Detlef-M. Smilgies, Dennis Nordlund, and Luisa Whittaker-Brooks*

Cite This: *ACS Appl. Polym. Mater.* 2021, 3, 2938–2949 Read Online

ACCESS | Metrics & More | Article Recommendations | Supporting Information

ABSTRACT: To close the technological gap between laboratory-based conducting polymers and commercially available inorganic semiconductors, it is imperative to develop synthesis approaches that allow for the fabrication of morphology-controlled polymers where charge carriers can be readily fine-tuned. Herein, our studies provide a detailed investigation of the polymerization protocols needed to afford the fabrication of well-defined and highly ordered polymer thin films. Using poly(3,4-ethylenedioxythiophene) (PEDOT) as a case study, we demonstrate strong correlations between the polymerization protocols and counterion dopants in driving the observed changes in crystallinity and π-stacking ordering of fabricated thin films. Upon the fabrication of thin films with controlled morphologies, we can provide an in-depth characterization of the thermoelectric properties (i.e., electrical conductivity, Seebeck coefficient, and power factor) of doped PEDOT chains as a function of counterion dopants and oxidation levels. Given the high power factors, we fit the thermoelectric characteristics of our samples to determine the charge transport mechanism in PEDOT thin films as a function of polymerization protocols and counterion dopants. On the basis of the fits, we report record-breaking transport function values which are indicative of bandlike transport in PEDOT thin films. As such, these high transport function values may point to the fabrication of well-defined and highly conducting polymers that can achieve thermoelectric figure of merit values above 0.6 at room temperature.

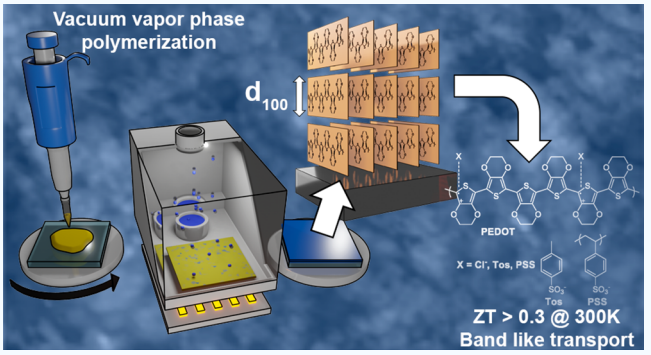

KEYWORDS: *PEDOT, polarons, oxidation level, thermoelectric properties, NEXAFS*

INTRODUCTION

The dawning of the organic electronics field can be rooted back to 1977 when Alan J. Heeger, Alan G. MacDiarmid, and Hediki Shirikawa pioneered the discovery and development of conducting polymers.[1,2] Such discovery quickly reshaped the organic electronics field and prompted many researchers to investigate new synthesis and doping approaches to yield high performing conducting polymers beyond polyacetylene.

A conducting polymer is typically composed of a π-conjugated backbone that in its pure state is insulating. This π-conjugated backbone can be treated with either a reducing or an oxidizing agent to induce the generation of charge carriers. Upon their generation, charge carriers delocalize throughout the π-conjugated backbone, thus inducing an increase in the electrical conductivity of the polymer that is comparable to that observed in metallic systems. Also, the addition of a counterion after treating the polymer with a reducing or oxidizing agent is needed to achieve charge neutrality.[3−5]

Several conducting polymers such as polyaniline (PANI), polypyrrole (PPY), poly(*p*-phenylenevinylene) (PPV), polythiophene (PTh), and poly(3,4-ethylenedioxythiophene) (PEDOT) derivatives have attracted tremendous attention and have become textbook examples due to their high electrical conductivity ($1-10^3$ S cm^{-1}), reversible doping−dedoping mechanism, tunable chemical and optoelectronic properties, ability to be cast into flexible thin films and form factors, and ease of processability. Regardless of the nature of the π-conjugated backbone comprising these conducting polymers, extrinsic dopants and counterions need to be introduced to modify their electrical properties.[6] The addition of dopants and counterions introduces structural disorder that could detrimentally affect the electrical properties of conducting polymers. As charge transport in conducting polymers is directly dependent on π-conjugation, the observed electrical conductivity may be inherently anisotropic.[7] Therefore, further understanding of the role that dopant structure,

Received: January 16, 2021
Accepted: May 5, 2021
Published: May 11, 2021

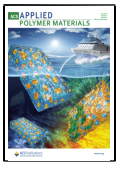

counterions, and polymerization protocols of conducting polymers has on their morphology and electronic structure is warranted. However, this is not an easy task to tackle given that morphology and electronic structure changes as a function of dopant structure, counterions, and polymerization methods are often convoluted.

Specifically, to PEDOT, its conducting nature can be achieved via the polymerization of EDOT monomers followed by redox doping. To balance the positively charged oxidized PEDOT molecule, the redox doping process is performed in the presence of negatively charged molecular counterions such as polystyrenesulfonate (PSS^-) and tosylate (Tos^-) or halide ions such as Cl^- (Figure 1A).[8−11] All these counterions impart different morphology, stability, and alignment of the oxidized PEDOT chains which ultimately affect charge carrier generation and propagation.[12−14] Research into the optimization methods for polymerization and counterion selection has shown promising results in controlling the thermoelectric parameters in PEDOT thin films. This has included exchanging counterions and the use of solvent treatments to control the oxidation level.[10,15−17]

Charge carriers in PEDOT can be found as polarons or bipolarons depending on the PEDOT:counterion complex and its doping level.[18,19] Modulation of the charge carriers has resulted in electrical conductivities (σ) of 2500 S cm^{-1} for PEDOT:PSS thin films post-treated with H_2SO_4.[20] The σ can be further improved to 3400 S cm^{-1} when Tos^- is used as the counterion.[21] The intrinsic dopant trifluoromethanesulfonate (OTf) counterions have shown an even higher conductivity of 3600 S cm^{-1}, which has been further enhanced to 5400 S cm^{-1} by replacing the OTf with a hydrogenosulfate counterion through extrinsic treatment.[22] Because of its high electrical conductivity coupled with its low work function (4.3 eV) and high ionic mobility (2.2×10^{-3} cm^2 V^{-1} s^{-1}), PEDOT has been extensively investigated as source and drain electrodes in electrochemical transistors and ion pumps,[23,24] beyond indium tin oxide (ITO) electrode replacements in photovoltaic devices,[25] as a cathode material in electrolytic capacitors,[26] and as an efficient waste-heat recovery (i.e., thermoelectric) material.[15,27] Beyond the potential applications of PEDOT, we can use its waste-heat recovery properties to generate fundamental insights into how dopant structure, counterions, and polymerization protocols affect polymeric systems.

The waste-heat recovery properties of a material are quantified by the dimensionless thermoelectric figure of merit, ZT. This is defined as $ZT = S^2\sigma T/\kappa$, where S is the Seebeck coefficient, σ is electrical conductivity, T is the absolute temperature, and κ is the thermal conductivity. Ideally, a good thermoelectric material will behave differently for electrons and phonons, acting as a glass to phonons and a crystal to electrons, thus scattering phonons and allowing electrons to readily diffuse throughout a device. Given the intrinsically low κ of PEDOT (0.2−0.6 W m^{-1} K^{-1}), it is possible to achieve ZT values ranging from 0.25 to 0.42 at room temperature.[15,28,29] Despite multiple efforts, achieving a reproducible high ZT for PEDOT thin films is often challenging. We believe this stems from the lack of fundamental understanding of their electronic structure and morphology as a function of polymerization protocols and counterions. In terms of the electronic structure, PEDOT can be treated as a semiconductor with a transport edge and shape factor. This gives us an empirical relationship between σ and S that allows us to gain insight into the charge carrier

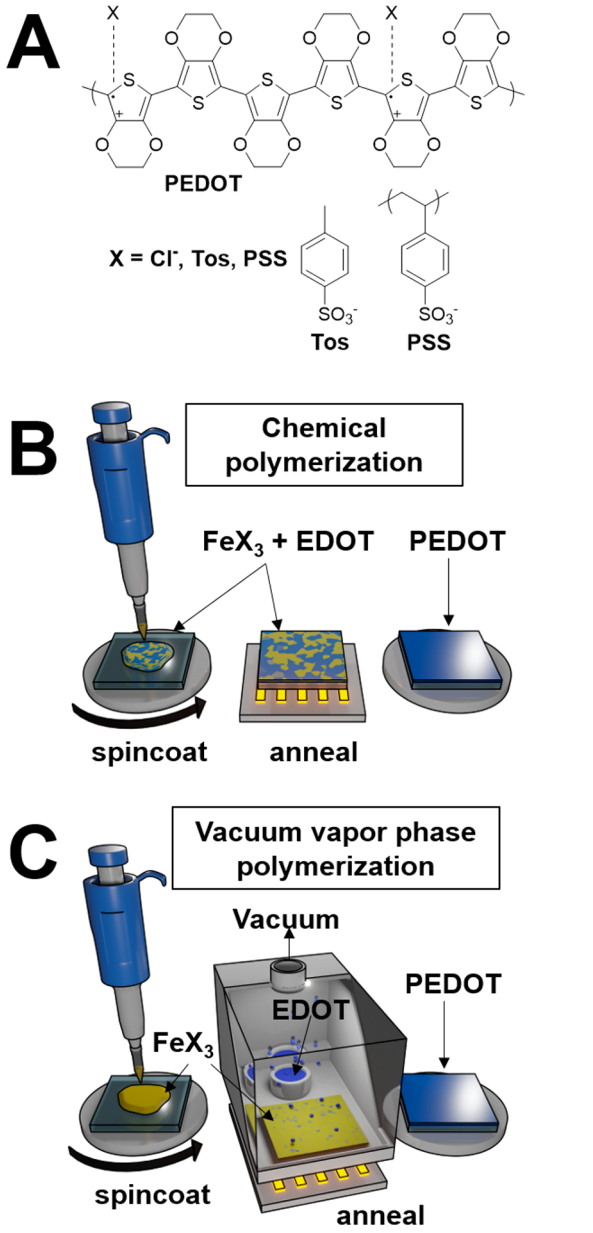

Figure 1. (A) Chemical structure for PEDOT with intrinsic charge carriers counterbalanced by X, where X = Cl^-, Tos^-, or PSS^-. (B) Depiction of the chemical polymerization (CP) process where the oxidant FeX_3 is mixed and spin-coated with the monomer EDOT and annealed to form PEDOT films. (C) Depiction of the vacuum vapor phase polymerization (VVPP) process where the oxidant is spin-coated onto a substrate and placed under vacuum and heated with EDOT, which can interact with the oxidant as a vapor and diffuse into the film.

distribution. Thus, it can be inferred that the thermoelectric characteristics of PEDOT are governed by the transport coefficient σ_0. Understanding and modulating the morphology, counterions, and polymerization parameters that affect σ_0 will allow for the design of highly oriented PEDOT thin films with remarkable electronic properties. To date, most reports have demonstrated that the σ_0 can be enhanced upon the formation of polarons/bipolarons via postpolymerization treatment of PEDOT thin films.[30,31] However, postpolymerization treatments can also induce structural strain and heterogeneities which can impact the electrical properties of PEDOT thin

https://doi.org/10.1021/acsapm.1c00069
ACS Appl. Polym. Mater. 2021, 3, 2938−2949

films.[32,33] Many efforts have been devoted to developing prepolymerization protocols to circumvent the structural strain and poor control over the morphology of PEDOT thin films subjected to postpolymerization treatments. Although postpolymerization protocols are effective for the fabrication of highly conducting PEDOT thin films, there is still a need to decouple the individual contributions of the counterions and the type of prepolymerization methods on the overall morphology and electrical properties of PEDOT thin films.

Using PEDOT thin films as a case study, we herein investigate (1) the morphological changes imparted by the dopant structure and counterions as a function of polymerization methods, (2) the nature of the electronic structure of PEDOT in terms of its thermoelectric properties (i.e., electrical conductivity, Seebeck coefficient, and power factor), and (3) the nature of charged states (i.e., bipolaron vs polarons). Our findings provide key insights into the role that polymerization protocols and counterions play in modifying the morphology and electronic structure of PEDOT. We believe this fundamental understanding can be utilized for promoting the design, synthesis, and device assembly of conducting polymeric thin films beyond PEDOT.

EXPERIMENTAL SECTION

Chemical Polymerization (CP) of PEDOT:X Thin Films. The 1 in. × 1 in. glass substrates were cleaned in sequentially sonicated baths of soapy water, DI water, acetone, and isopropyl alcohol. Following sonication, substrates were also oxygen plasma cleaned for 10 min. Each sample was pre-etched on the backside of the glass to break into four 1 in. × 1/4 in. films with one piece broken an additional time into two 1/2 in. × 1/4 in. films to perform all characterization on a single film. CP syntheses were performed by using a solution containing either iron(III) tris(*p*-toluenesulfonate) ($FeTos_3$) (0.4 M) or iron(III) chloride ($FeCl_3$) (0.4 M) and the triblock copolymer PEG:PPG:PEG (MW 5700) (47 M) in butanol. Solutions were heated to 40 °C and stirred for 6 h to achieve homogeneity. Subsequently, the monomer 3,4-ethylenedioxythiophene (EDOT) was added to the solutions under sonication in a 1:5 monomer-to-oxidant solution volumetric ratio. Once carefully mixed, 250 μL solutions were spun-cast at 4500 rpm for 30 s to create thin films atop the cleaned glass substrates. The PEDOT polymer with either a Tos^- or Cl^- counterion dopant formed as the spun-cast films were annealed at 70 °C for 2 h. Any iron(III) precursor residue was then removed from the film by using three sequential ethanol rinses.

Vacuum Vapor Phase Polymerization (VVPP) of PEDOT:X Thin Films. A homogeneous solution containing either $FeTos_3$ (0.25 M) or $FeCl_3$ (0.25 M) along with the triblock copolymer PEG:PPG:PEG (MW 5700) (45 M) in butanol was spun-cast (250 μL) atop clean glass substrates at 1500 rpm for 25 s. The resulting films were annealed at 70 °C for 10 min before being placed inside an airtight sealed chamber with a solution (500 μL) of the monomer EDOT. Samples were left under ∼45 mbar at 45 °C for 20 min, allowing EDOT to interact with the film surface as a vapor and diffuse toward the glass during polymerization. Upon removal, the thin film was annealed at 70 °C for an additional 10 min and subsequently rinsed in three sequential ethanol rinses.

Characterization. Surface morphology, including domain sizes and roughness for the PEDOT thin films, was characterized by using a Bruker Dimension Icon atomic force microscope (AFM) operated in the automated scan assist. Thin film thicknesses were also determined by using an AFM. Here, a segment of the thin film was scratched away, and a step height difference between the glass and the polymer layers was measured. The glass height was measured by fitting a line to the flat floor signal, while the polymer surface height was measured by using an average height away from the taller ridge observed during scraping. Confocal Raman spectroscopy was conducted by using a WiTec instrument for confocal micro-Raman spectroscopy. This setup uses a solid-state sapphire SF laser. The excitation wavelength was 488 nm. The output power was adjusted to 10 mW over a nominal spot size of 610 nm. GIWAXS data were collected at the Cornell High Energy Synchrotron Source Laboratory (CHESS, beamline D1). The X-ray beam energy was kept at a constant 10.5 keV with the beam aligned at a grazing angle of 0.18° with respect to the substrate. The scattered intensity was collected with a Pilatus 200l pixel array detector comprising 487 × 407 pixels with a size of 0.172 mm. The sample-to-detector distance was 170 mm. To limit issues with geometric smearing of the peaks on the detector, the width of the samples in the direction of the beam was kept to 0.5 cm. All GIWAXS images were background subtracted, and polarization and absorption corrections were applied, though these corrections were generally small. All GIWAXS images and linecuts were processed by using the graphical user interface GIXSGUI.[34] The mosaicity factor (MF) for each sample was computed by using the MATLAB code ShekieFactor.m. This code allows for an efficient method to quickly extract MF information from azimuthal linecuts of GIWAXS data.[35] Raman spectra were acquired by using a Jobin-Yvon Horiba Labram HR instrument coupled to an Olympus BX41 microscope with 632.8 nm laser excitation from an Ar-ion laser. An 1800 lines/mm grating was used to acquire spectra yielding a spectral resolution greater than 2 cm^{-1}. Raman spectra were acquired for 300 s intervals. The laser power was kept below 300 μW to minimize local heating.

To investigate the oxidation and chemical environments of the PEDOT thin films, X-ray photoelectron spectroscopy (XPS) studies were performed. XPS spectra were acquired by using a Kratos Axis Ultra DLD equipped with a hemispherical analyzer and an Al Kα (1486.6 eV) source. A pass energy of 160 eV was used for survey scans, while a 40 eV pass energy was used for detailed scans. All measurements were performed at normal take-off angles. The acquired spectra were standardized by calibrating against the adventitious carbon peak at 284.8 eV. Ultraviolet photoelectron spectroscopy (UPS) studies were performed by using a HeI (21.22 eV) excitation line of a He plasma in a discharge lamp. Spectra were taken at a pass energy of 5 eV for a nominal experimental resolution smaller than 150 meV. Curve fitting was performed by using CasaXPS software with a Gaussian−Lorentzian product function. The full width half-maximum (fwhm) was restricted to 0.7−3 eV, and a nonlinear Shirley background type was used for all peaks observed.

The electronic structure of PEDOT thin films was studied by C K-near-edge X-ray absorption fine structure (NEXAFS) spectroscopy measurements performed at the Stanford Synchrotron Radiation Lightsource (SSRL, beamline 10-1). A variable line spacing plane grating monochromator using a 600 lines/mm grating with a nominal energy resolution of ∼0.1 eV was used for the acquisition of all the C K-edge spectra. The spectra were acquired in partial electron yield mode by using a channeltron electron multiplier located near the sample with the detector at an entrance grid bias of −200 V to enhance surface sensitivity. A charge compensation gun was used to avoid sample charging. A carbon mesh was used as a reference standard for calibration of the energy scale for each spectrum by using the π^* transition at 285 eV. To eliminate the effects of incident beam intensity fluctuations and monochromator absorption features, the partial electron yield signals were normalized by using the drain current of a freshly evaporated gold mesh with 90% transmittance located along the path of the incident X-rays. All data were acquired at magic angles (θ = 54.7°). All spectra were pre- and postedge normalized to unity for direct comparison. Seebeck measurements were conducted on a custom-built instrument consisting of four K-type thermocouples arranged in a four-point probe configuration. The two inner thermocouples were used to measure the temperature gradient by using a National Instruments NI-9213 DAQ card while a voltage bias was measured across the sample by using two Keithley 2182A nanovoltmeters. The Seebeck coefficient of each film was measured by using a temperature difference of 10 °C. Electrical conductivity measurements were conducted by using an Ecopia HMS-5000 Hall testing system. The electrical conductivity for each sample was further corroborated by using the home-built Seebeck/electrical conductivity measurement instrument in a four-point probe

https://doi.org/10.1021/acsapm.1c00069
ACS Appl. Polym. Mater. 2021, 3, 2938−2949

configuration. Here, a Keithley 6220 was used to provide a DC source along with the Keithley 2182A nanovoltmeters. All sample thicknesses used to determine the sheet electrical conductivity were determined via AFM measurements.

RESULTS AND DISCUSSION

The morphology and electrical properties of PEDOT thin films can be controlled by modulating both the polymerization methods and the oxidation level of the PEDOT chains upon changes to the counterion structure. PEDOT thin films can be prepared by following a chemical polymerization (CP) or a vacuum vapor phase polymerization (VVPP) approach. As displayed in Figure 1B, the fabrication of PEDOT thin films via the CP approach involves the spin-coating and subsequent annealing of a homogeneous solution containing the monomer EDOT. An iron(III)-based oxidant (FeX_3) can also be added to the solution containing the monomer to afford charge balanced and doped PEDOT:X thin films. Here, X is either a tosylate (Tos^-) or a chloride (Cl^-) counterion. Alternatively, the fabrication of PEDOT thin films can be achieved by using a VVPP approach that involves spin-coating a solution of FeX_3 onto a substrate and annealing the film in a vacuum-sealed chamber (≈45 mbar) containing the monomer EDOT. Upon raising the temperature, EDOT will sublime and diffuse into the film covered with the oxidant counterion (Figure 1C). Such a process will induce the polymerization of EDOT into PEDOT. The fabrication of PEDOT thin films employing CP and VVPP approaches is used to investigate the role that morphology plays in tuning their electrical properties. We also modify the oxidation levels of PEDOT upon the incorporation of Tos^- and Cl^- counterion dopants to investigate their role in tuning the electrical properties of our thin films.

Atomic force microscopy (AFM) experiments were conducted to investigate the surface morphology of PEDOT thin films as a function of polymerization protocols and counterions. Figure 2 depicts the height AFM images for CP PEDOT:Cl, VVPP PEDOT:Cl, CP PEDOT:Tos, and VVPP PEDOT:Tos thin films. PEDOT:Cl thin films fabricated via the CP approach display the highest surface roughness (r_q) value with an average r_q of 72.6 nm (Figure 2A). In contrast, PEDOT:Cl thin films prepared by using the VVPP approach show a drastic decrease in surface roughness with an average r_q of 6.3 nm (Figure 2B). When Cl^- counterions are replaced by Tos^- counterions in PEDOT thin films prepared by using the CP approach, we observe that the films have a much lower surface roughness with an r_q of 14.2 nm (Figure 2C). Interestingly, PEDOT:Tos thin films prepared via the VVPP approach have the lowest surface roughness with an average r_q of 3.1 nm (Figure 2D). Overall, we can infer that the VVPP fabrication approach yields smoother films when compared to the CP fabrication approach. Similarly, upon comparison of the effect of counterion selection, the surface domain size and roughness are smaller when PEDOT chains are balanced with Tos^- over Cl^- counterion dopants. AFM was also used to determine the thickness of each the PEDOT films (Figure S1).

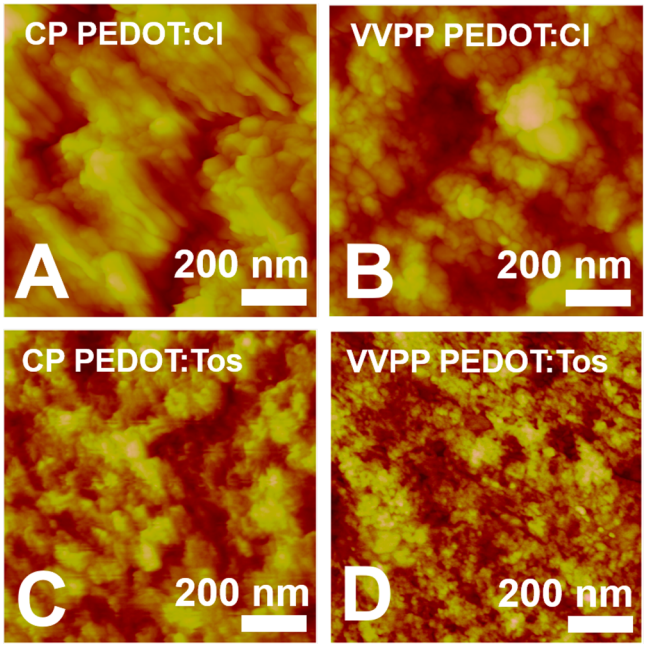

Figure 2. AFM images for PEDOT:Cl thin films prepared following the CP (A) and VVPP (B) fabrication approaches. PEDOT:Tos thin films prepared via the CP (C) and a VVPP (D) fabrication methods.

Insights into the nature of the carbon−carbon bonding present in the PEDOT structure as a function of polymerization environments and counterion dopants can be obtained from Raman spectroscopy studies. Figure 3A shows the Raman spectra for CP PEDOT:Cl, VVPP PEDOT:Cl, CP PEDOT:Tos, and VVPP PEDOT:Tos thin films. As depicted, all samples exhibit vibration bands appearing at ∼1365, ∼1433, and ∼1508 cm^{-1} which may be ascribed to $C_\beta{=}C_\beta$, $C_\alpha{=}C_\beta$, and asymmetric $C_\alpha{-}C_\beta$ stretching modes, respectively.[36,37] Our Raman studies also demonstrate that there are significant conformational changes of the PEDOT chains that are induced either by the polymerization method or the counterions. To provide some perspective, in a neutral PEDOT chain structure, the dominant $C_\alpha{=}C_\beta$ stretching mode is centered around ≈1452 cm^{-1}. This stretching mode is characteristic of a PEDOT structure comprising a thiophene core with a benzoidal character. As the PEDOT chains are oxidized and doped, the dominant $C_\alpha{=}C_\beta$ stretching mode red-shifts to ≈1423 cm^{-1} and is indicative of the PEDOT chains having a quinoidal character. The observed conformational changes, as characterized by variations of the $C_\alpha{=}C_\beta$ stretching mode of

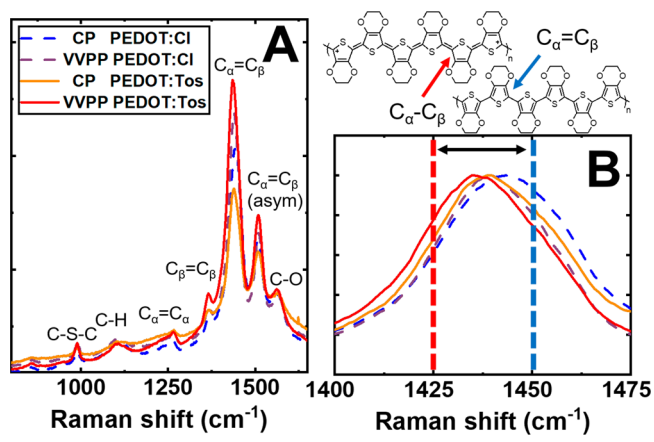

Figure 3. Raman spectra for PEDOT thin films as a function of polymerization method and counterion dopant. Major vibration modes are depicted in (A) for clarity. (B) High-resolution scan around the $C_\alpha{-}C_\beta$ and $C_\alpha{=}C_\beta$ vibration modes for the investigation of the benzoidal and quinoidal structures, respectively. Laser excitation wavelength: 632.8 nm.

https://doi.org/10.1021/acsapm.1c00069
ACS Appl. Polym. Mater. 2021, 3, 2938−2949

the thiophene core, can serve as footprints to qualitative determine the oxidation level of the PEDOT chains and hence the degree of doping of the thin films. As depicted in Figure 3B, there are striking differences in the $C_\alpha{=}C_\beta$ stretching mode of the thiophene core of the PEDOT structure as a function of polymerization methods and counterions. Here, the $C_\alpha{=}C_\beta$ stretching mode for CP PEDOT:Cl appears at maxima of 1443.8 cm^{-1}, and it is the sample having the most benzoidal character. This is followed by VVPP PEDOT:Cl with a maximum of 1439.9 cm^{-1}. Upon charge balancing the PEDOT chains with Tos^- counterions, the $C_\alpha{=}C_\beta$ stretching mode for CP PEDOT:Tos is slightly red-shifted to a maximum of 1438.6 cm^{-1}. Remarkably, when PEDOT is doped with Tos^- counterions via the VVPP polymerization approach (VVPP PEDOT:Tos), the $C_\alpha{=}C_\beta$ stretching mode appears at a maximum of 1434.8 cm^{-1}. Thus, VVPP PEDOT:Tos is the sample with the thiophene core exhibiting the most quinoidal character. From the Raman studies, we can then infer that the CP fabrication approach yields conducting polymer thin films with lower oxidation and doping levels when compared to the VVPP fabrication approach. Also, when comparing the structural effects imparted by the Cl^- and Tos^- counterions on PEDOT thin films prepared by using the same polymerization protocol (e.g., VVPP), we can infer that using Tos^- as the counterion promotes the formation of highly doped PEDOT thin films.

Further insight into the doping level for each PEDOT thin film as a function of polymerization methods and counterions can be obtained by determining the distribution widths of the $C_\alpha{=}C_\beta$ stretching mode along the thiophene core. The distribution width for each Raman vibration mode can be characterized by using a Gaussian distribution (P_G) which can be formulated in terms of the mean (μ) and the standard deviation (StdDev) as per the following equation:

$$P_G(x) = \frac{1}{\sqrt{2\pi}\,\mathrm{StdDev}} e^{-(x-\mu)^2/2\mathrm{StdDev}^2} \quad (1)$$

where x is the vibration mode location in wavenumbers and μ describes the mean value of the Gaussian, in this case the maxima. Here, the resultant σ describes differences in the distribution width. The σ for PEDOT:Cl prepared via the CP method is 15.0 cm^{-1}, while that for PEDOT:Cl prepared by using the VVPP method is 13.6 cm^{-1}. The narrower distribution of vibrational states in VVPP PEDOT:Cl suggests a higher density of doping states within the thin film when compared to CP PEDOT:Cl. A similar trend is observed for PEDOT:Tos where StdDev is slightly narrower for thin films prepared by using the VVPP method (14.1 cm^{-1}) than that of the CP method (14.4 cm^{-1}). These differences in StdDev show that the distribution of quinoidal to benzoidal states is much tighter for films prepared by using VVPP when compared to that of the CP method.

The morphology and structure of the PEDOT thin films were investigated via grazing incidence wide-angle X-ray scattering (GIWAXS) studies. Figure 4 shows indexed 2D GIWAXS images for PEDOT thin films as a function of the polymerization methods and counterions. All GIWAXS profiles contain crystallographic reflections associated with the {h00} family of planes which is a clear indication of the semicrystalline nature exhibited by all the samples. However, the degree of crystallinity and crystallite orientation vary from sample to sample. For instance, the crystallographic reflections associated with the {h00} family of planes observed in the GIWAXS

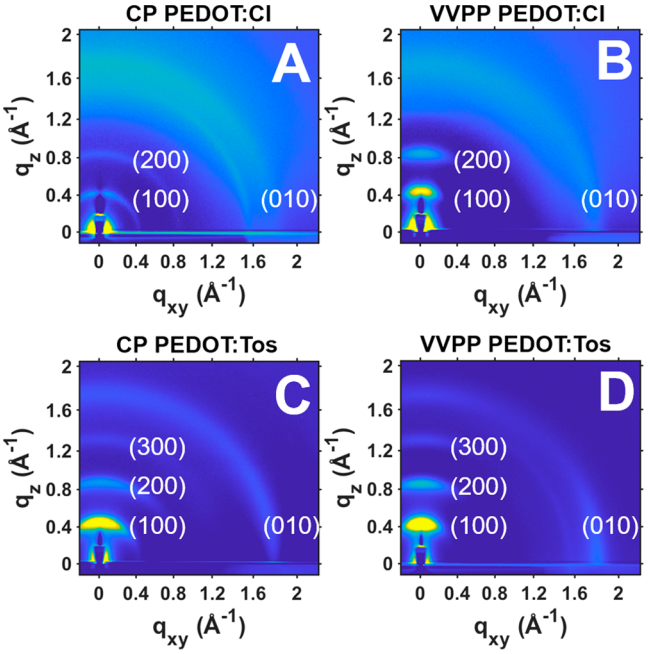

Figure 4. GIWAXS patterns for CP PEDOT:Cl (A), VVPP PEDOT:Cl (B), CP PEDOT:Tos (C), and VVPP PEDOT:Tos (D) thin films. For clarity, we have labeled the crystallographic planes associated with lamellae {h00} and $\pi{-}\pi$ stacking (010) of PEDOT chains.

profile for CP PEDOT:Cl thin films show an overall lack of orientation. Interestingly, there is an anisotropic azimuthal distribution of the crystallographic reflections associated with the {h00} family of planes in the VVPP PEDOT:Cl thin film. To our knowledge, VVPP is the first reported polymerization protocol that yields any favorable orientation for a PEDOT thin film containing Cl^- as the counterion. Similarly, we observe a narrower anisotropic azimuthal distribution of the crystallographic reflections associated with the {h00} family of planes for VVPP PEDOT:Tos when compared to CP PEDOT:Tos. Further analysis of the GIWAXS profiles suggests that the polymerization method used for the fabrication of PEDOT:Cl and PEDOT:Tos plays a major role in driving the favorable out-of-plane orientation of crystallites within a thin film as well as the crystallinity. As depicted in Figure 4, the GIWAXS profiles suggest that the VVPP fabrication approach yields thin films that are more semicrystalline and anisotropically oriented out-of-plane with respect to the substrate. In terms of the counterion, PEDOT thin films having Tos^- as compared to ones with Cl^- are significantly more semicrystalline and anisotropically oriented out-of-plane with respect to the substrate.

Furthermore, the azimuthal linecuts of the (200) crystallographic plane shown in Figure 5A highlight the differences in crystallite orientation for PEDOT thin films being subjected to different polymerization methods and counterions. To understand the differences in crystallite orientations, we calculated the mosaicity factor (MF) based on the azimuthal linecuts of the (200) crystallographic plane for each sample.[35] The MF can be determined by using the following equation:

$$\mathrm{MF}_{(hkl);\varphi_s}(\varphi) = \sum A_w(\varphi) S_{\varphi_s}(\varphi) = \frac{A_\varphi}{\sum \mathrm{A}} \frac{45 - |\varphi_s - \varphi|}{45} \quad (2)$$

https://doi.org/10.1021/acsapm.1c00069
ACS Appl. Polym. Mater. 2021, 3, 2938−2949

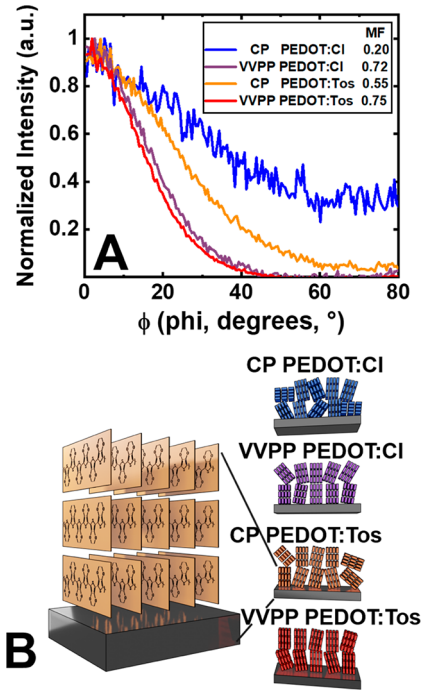

Figure 5. (A) Normalized intensity of the (200) crystallographic plane of PEDOT plotted as a function of Φ, the azimuthal angle measured along q_z = 0. (B) Cartoon depicting the crystallite arrangements of PEDOT with respect to the glass substrate as a function of polymerization growths and counterion dopant.

where φ_s is the azimuthal angle of interest, A_w is the weighted amplitude of crystallographic signal intensity, and S_{φ_s} is a linear transformation that weights values relative to any angle of interest. MF allows for the orientation of crystallites within a thin film to be compared on a linear scale of 1 to −1. A Miller index reflection plane with an MF value of 1 corresponds to a crystal plane that is perfectly oriented along the q_z diffraction plane (φ = 0°) or out-of-plane with respect to the sample substrate, while a value of −1 corresponds to perfect orientation along φ = 90°. A reflection with an MF value of 0 corresponds to randomly disordered crystallites with respect to the substrate. As shown in Figure 5A, CP PEDOT:Cl exhibits a broader distribution of crystallites with an overall $MF_{(200)}$ = 0.20, and it is the least oriented sample in the series. The crystallite orientation distribution significantly narrows and becomes more azimuthally anisotropic in thin films based on VVPP PEDOT:Cl with a calculated $MF_{(200)}$ = 0.72. Even more so, VVPP PEDOT:Tos thin films are more oriented along the q_z plane with a $MF_{(200)}$ = 0.75 when compared to CP PEDOT:Tos thin films ($MF_{(200)}$ = 0.55). On the basis of the overall MF values, we can draw a schematic depiction of how the crystallites within the PEDOT thin films are oriented relative to the substrate. As depicted in Figure 5B, PEDOT:Cl thin films fabricated by using the CP method (blue) are composed of crystallites mostly randomly oriented along the substrate with a small fraction of crystallites oriented out-of-plane. There is a slight increase in crystallite orientation when PEDOT:Cl thin films are prepared via the VVPP approach (yellow). Furthermore, crystallites within the PEDOT thin films are significantly more oriented when Tos^- is used as the counterion and VVPP is used as the fabrication method (red) when compared to thin films prepared via the CP approach (purple). Combining both the Raman and GIWAXS results, we can conclude that the counterion selection drives the overall structural doping while the judicious choice of a polymerization protocol allows for the morphology to be controlled. Upon controlling the morphology, it is possible to tune the doping level within the thin film. Moreover, as our results indicate, the VVPP fabrication approach often yields highly oriented thin films with well-controlled morphologies and doping levels. However, as a caveat, the VVPP fabrication approach is diffusion-limited as well as kinetics-limited and highly depends on how the polymerization precursors are transported throughout the film.[38] Therefore, to avoid vertical inhomogeneities of the counterion dopant as well as the PEDOT chains, it is necessary to ensure that the monomer is given enough time to react with the counterion dopant precursor.

Given that variations in morphology are often associated with changes in carrier density and doping level in conducting polymers,[10,39] we performed X-ray photoelectron spectroscopy (XPS) studies to investigate the chemical environments and oxidation states in our PEDOT thin films as a function of processing conditions and counterion dopants. All XPS survey scans depicted in Figure S2 confirm the absence of any precursor impurities (e.g., $FeCl_3$ or $FeTos_3$) as well as the presence of Cl exclusively in the PEDOT:Cl thin films. A high-resolution scan for the S 2p region is presented in Figure 6A. All PEDOT thin films show a spin-split doublet consisting of S $2p_{1/2}$ and S $2p_{3/2}$ from 165.6 to 163.4 eV which is characteristic of the thiophene backbone. When Tos^- is used as the counterion, we observe a new sulfur environment from 169.5 to 166.6 eV. The binding energy of the sulfur electron in Tos^- is higher than that of the sulfur electron in the thiophene backbone because of the increased electronegativity around the sulfur atoms in the Tos^- counterion dopant.[40−42] Furthermore, there is a blue-shift of ∼0.2 eV in the sulfur binding energy around the thiophene core when Tos^- is added as the counterion in PEDOT over Cl^-. This blue-shift is indicative of a molecular rearrangement of the PEDOT chains induced by the counterion dopants due to screening of the bound electrons from the thiophene core.

Because the counterion dopants are introduced to achieve charge neutrality of the PEDOT chains, we can therefore determine the charge density of the polymer thin films by quantitatively fitting the XPS spectra (Figure S3). The charge density for PEDOT:Cl (which is correlated to the oxidation level of the film) can be calculated by obtaining the ratio of the integrated areas of the low binding energy of the Cl $2p_{1/2}$ and Cl $2p_{3/2}$ to the high binding energy of the S $2p_{1/2}$ and S $2p_{3/2}$ from the thiophene core. Similarly, the charge density for PEDOT:Tos can be calculated by obtaining the ratio of the integrated areas of the low binding energy of the S $2p_{1/2}$ and S $2p_{3/2}$ from the Tos^- group to the high binding energy of the S $2p_{1/2}$ and S $2p_{3/2}$ from the thiophene core. The oxidation of CP PEDOT:Cl is calculated to be ≈26%, or 1 Cl^- for 3.8 EDOT repeat units. Conversely, we observed an increase in the oxidation level of PEDOT:Cl to ≈37% (1 Cl^- for 2.7 EDOT repeat units) when the films are fabricated following the VVPP approach. When we replace Cl^- from Tos^-, an oxidation level of ≈38% (1 Cl^- for 2.6 EDOT repeat units) is calculated for CP PEDOT:Tos, while an oxidation level of ≈44% (1 Cl^- for 2.3 EDOT repeat units) is calculated for VVPP PEDOT:Tos thin films. From these results, we can therefore infer that (1) the VVPP approach allows for the fabrication of PEDOT thin films with a higher doping

https://doi.org/10.1021/acsapm.1c00069
ACS Appl. Polym. Mater. 2021, 3, 2938−2949

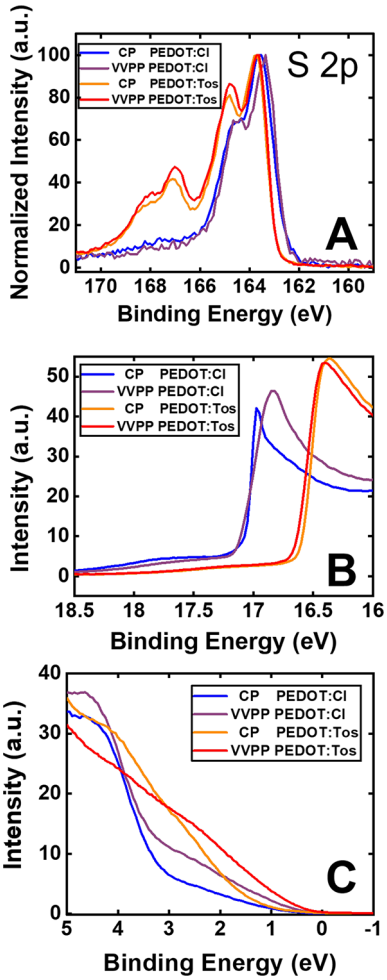

Figure 6. Chemical environment, work function, and density of valence electronic states for PEDOT thin films as a function of polymerization approaches and counterion dopants. (A) XPS spectra of the S 2p region. (B) Secondary electron cutoff energy region of the UPS spectra. (C) UPS low binding energy region near the ε_f.

oxidation level and (2) introduction of Tos^- counterions over Cl^- increases the number of charge carriers present within the thin films.

The work function and the density of valence electronic states for the PEDOT thin films as a function of polymerization approach and counterion dopants can be elucidated via ultraviolet photoelectron spectroscopy (UPS) studies. The secondary electron cutoff energy (E_{SECO}) region for all PEDOT thin films is provided in Figure 6B. The work function can be calculated by subtracting the E_{SECO} from a HeI photon source (21.22 eV). The work function for CP PEDOT:Cl is calculated to be 4.12 eV, while VVPP PEDOT:Cl is calculated to be slightly lower at 4.06 eV. A similar trend is observed when Tos^- is used as the counterion, with CP PEDOT:Tos having a work function of 4.60 eV while VVPP PEDOT:Tos thin films have a slightly lower work function of 4.55 eV. Interestingly, this shows that PEDOT:Cl has a lower work function when compared to PEDOT:Tos by nearly 0.50 eV in both polymerization methods.

The UPS low binding energy region for all PEDOT thin films is depicted in Figure 6C. This region provides information into the density of valence electronic states associated with the π electrons present in the thiophene backbone of the PEDOT structure.[41,43,44] It is also worth noting that only π electrons contribute to the signal in the lower binding energy range near the Fermi edge (ε_f). As illustrated in Figure 6C, the UPS low binding energy spectra for CP PEDOT:Cl and VVPP PEDOT:Cl thin films are composed of two different components, i.e., a sharp decay feature at 3.0 eV and a tail extending into the ε_f. In contrast, the UPS low binding energy spectra for CP PEDOT:Tos and VVPP PEDOT:Tos thin films show a much broader tail. Because of an increase in the oxidation level, the electronic structure of the resulting PEDOT chains is distorted, further promoting the evolution of these tails all into the Fermi energy level (ε_f). These tails are associated with the presence of localized filled states induced by disorder.[10] Hence, the observed larger intensity of these tails would suggest a higher density of states in the PEDOT thin films. As shown in Figure 6C, CP PEDOT:Cl thin films have the lowest density of states near the ε_f whereas VVPP PEDOT:Tos thin films have the highest density of states near the ε_f. This further supports the premise that the structural and morphological changes to PEDOT are fairly drastic when exchanging the counterion as well as the polymerization protocol, which will ultimately determine the electrical properties of the PEDOT thin films.

In terms of the electronic structure, PEDOT thin films can be composed of highly ordered regions with extended $\pi-\pi$ stacking. These ordered domains may be separated by regions with a large degree of disorder.[45] In the disordered regions, the electronic structure can generally be treated as a variable array of molecular orbitals with discrete HOMO and LUMO energy levels, where the barrier for charge transport depends on the barrier for quantum tunneling between adjacent orbitals. More structural disorder leads to a greater number of trap states in the material: regions where charge carriers are immobilized by energy barriers that impede their mobility. Highly ordered domains tend to form a more bandlike electronic structure due to supramolecular orbital mixing. On a materials scale, this may cause charge carriers to percolate the disordered regions between regions of high mobility. Developing a transport model that would permit the rational optimization of the carrier concentration is further complicated by the fact that electronic coupling, which is stronger in the ordered regions, induces localized polarizations at varying length scales and strengths and across separate domains, the nature of which may be highly sensitive to processing conditions. Empirical evidence has clearly shown that charge transport does not follow a single mechanism,[46] and recent work has shown that the different modes of carrier transport may limit the electrical properties of a given organic semiconductor.[47]

The electronic structure of PEDOT thin films as a function of polymerization methods and counterion dopants was investigated via near-edge X-ray absorption fine structure (NEXAFS) spectroscopy studies. NEXAFS spectroscopy is an element- and edge-specific analytical technique based on the excitation of core electrons to empty or partially filled states above the Fermi level. NEXAFS dipole selection rules give rise to a "searchlight effect" that provides spectroscopic fingerprint characteristics into the electronic structure and chemical bonding in crystalline and amorphous materials.[48−51] Figure 7 depicts the C K-edge NEXAFS spectra for PEDOT thin films acquired at magic angle (54.7°). Several characteristic signatures are immediately discernible such as a 1s → $\pi^*_{C=C}$ transition at 285.1 eV, a 1s → π^*_{C-S} transition identified at 287.2 eV, a 1s → σ^*_{C-H} transition at 288.7 eV, a 1s → σ^*_{C-C}

https://doi.org/10.1021/acsapm.1c00069
ACS Appl. Polym. Mater. 2021, 3, 2938−2949

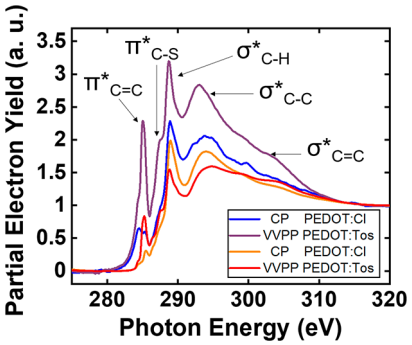

Figure 7. C K-edge spectra for PEDOT thin films as a function of polymerization methods and counterion dopants. All spectra have been pre- and postedge normalized to a unitary absorption cross-section to depict the relative spectral intensities.

transition at 293 eV, and a final broad transition state observed at 302 eV assigned to a 1s → $\sigma^*_{C=C}$ transition state.[49,52] NEXAFS spectra can exhibit dichroic sensitivity relative to the incident angle between the source and film surface, where a sample with the aromatic π^* signal oriented along a specific angle would only be excited when the X-ray is aligned with the polarity of the orbital.[53] Our NEXAFS spectra were collected at 55°, so care must be taken when discussing the observed orbital intensities, which when correlated to the GIWAXS data would suggest that these samples should display different orbital intensities at different experiment angles. Although the NEXAFS spectra for all PEDOT thin films, regardless of the polymerization method and counterion, have the mentioned transition states, they all show unique intensity features that allow us to find interesting trends. Before we further discuss these trends, it is important to note that NEXAFS probes empty orbitals[48,50] Hence, a decrease in intensity of a resonance or transition state, to a first approximation, corresponds to the occupation of states that give rise to the resonance. First, as depicted in Figure 7, the onset for the 1s → $\pi^*_{C=C}$ resonance occurs at a lower photon energy in PEDOT thin films prepared via the CP approach. This suggests that both the CP PEDOT:Cl and CP PEDOT:Tos thin films are composed of more nondiscrete electronic states which are indicative of a higher degree of conjugation. On the basis of the chemical structure for PEDOT, a higher degree of conjugation is expected for a structure with a benzoidal character. Second, we observe the splitting of the 1s → $\pi^*_{C=C}$ resonance at 285.1 eV. This splitting is due to the strong delocalization of the electronic structure along the conjugated backbone of the PEDOT structure. We also observe that the splitting of the 1s → $\pi^*_{C=C}$ resonance is more pronounced in the CP PEDOT:Cl, suggesting that this is the sample with the most delocalized states and benzoidal character among the series. Third, we observe various extents of intensities for the 1s → $\pi^*_{C=C}$ resonance at 285.1 eV. Changes in intensity of the 1s → $\pi^*_{C=C}$ resonance can be used to determine polaron formation. To the best of our knowledge, evidence of polaron formation and the accompanying geometric distortion in PEDOT by using NEXAFS have hitherto not been investigated. As shown, there is a prominent decrease in the relative intensity of the 1s → $\pi^*_{C=C}$ resonance for VVPP PEDOT:Cl, indicating the occupation of the lowest-lying conduction band states. This decrease in intensity also suggests a pronounced rehybridization of the C=C bonding as a result of a local structural distortion induced by exchange interactions and small polaron formation. In terms of structure, the formation of these polaronic states induces a quinoidal character in the PEDOT chains. Thus, it appears that the VVPP fabrication approach yields samples with a higher concentration of polaronic states when compared to the CP approach. We also hypothesize that the Cl^- and Tos^- counterion dopants are donating electron density to the PEDOT core that is being used to fill electronic states. It is important to mention that the decrease in the relative intensity of the 1s → $\pi^*_{C=C}$ resonance is nonmonotonic given the contribution of the C=C functional group of the tosylate structure to the signal. (There may also be a contribution from spectral anisotropy due to different molecular alignment and orientation of the polymer chains with respect to the polarized beam used for the NEXAFS experiments.) Finally, we observe a more pronounced shoulder at the 1s → π^*_{C-S} transition identified at 287.2 eV for the PEDOT thin films containing Tos^- as the counterion dopant. This is expected given the presence of a C−S bond in the Tos^- counterion as well as in the PEDOT structure. On the basis of these trends, we can then propose that polymer thin films prepared by using the VVPP method may have more localized electronic states that promote the formation of polaronic states.

To correlate morphology changes and electronic structure to electrical properties, we performed thermoelectric measurements that included the determination of the electrical conductivity (σ), the Seebeck coefficient (S), and the power factor (PF = $S^2\sigma$) for our PEDOT thin films. Figure 8A displays σ and S for PEDOT thin films as a function of polymerization protocols and counterion dopants. We determined a σ of 6.7 S cm^{-1} at room temperature for PEDOT:Cl thin films prepared by using the CP method. The σ of PEDOT:Cl can be further increased to 107.8 S cm^{-1} at room temperature by preparing the thin films by using the VVPP method. As the Cl^- counterion dopant is replaced by Tos^-, the PEDOT thin films become more conducting. The σ for CP PEDOT:Tos thin films is determined to be 144.0 S cm^{-1} while the σ for VVPP PEDOT:Tos thin films is 1027.3 S cm^{-1}. The σ observed in our PEDOT thin films is nicely correlated to morphology where the more oriented and crystalline thin films exhibit higher σ values.

When comparing the S for PEDOT thin films as a function of polymerization methods, we observe that the S for PEDOT:Cl thin films prepared via the CP approach is 17.0 μV K^{-1}. The S increases to 32 μV K^{-1} when PEDOT:Cl thin films are prepared by using the VVPP approach. However, we observe a different trend for PEDOT:Tos thin films where the S decreases from 85 μV K^{-1} for samples prepared via the CP approach to 65 μV K^{-1} for samples prepared via the VVPP approach. The fact that S is decreasing with increasing σ for VVPP PEDOT:Tos thin films may stem from the inverse interdependence of these two parameters with respect to charge concentrations within the sample. However, the PF for each film relays that increasing σ outweighs the losses over in the Seebeck coefficient (Figure 8B). The PF for PEDOT:Cl thin films increases from 0.194 to 11.0 μW m^{-1} K^{-2} when comparing samples prepared by using the CP to the VVPP method. The same trend is observed for PEDOT:Tos thin films where the PF increases from 104.0 to 434.0 μW m^{-1} K^{-2}. The PF obtained at room temperature for VVPP PEDOT:Tos thin films is on par with several high-performing inorganic thermoelectric materials as well as highly doped PEDOT thin films and Te-PEDOT heterostructures.[15,28,30,54,55] Moreover,

https://doi.org/10.1021/acsapm.1c00069
ACS Appl. Polym. Mater. 2021, 3, 2938−2949

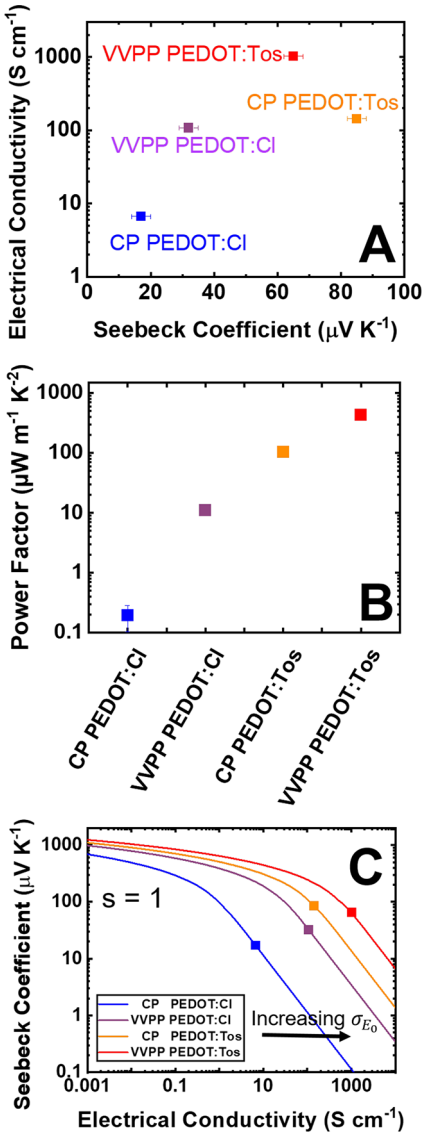

Figure 8. Thermoelectric properties of PEDOT films as a function of polymerization protocols and counterion dopants. (A) Electrical conductivity vs Seebeck coefficient. (B) Power factor. All measurements were acquired at 300 K. (C) Kang–Snyder transport model fit for the PEDOT thin films. All samples follow an $s = 1$ with increasing σ_{E_0}.

the high PF obtained for VVPP PEDOT:Tos thin films closes a gap between traditional inorganic thermoelectrics whose interrelated properties require that as the electrical conductivity of the material increases, the Seebeck coefficient must decrease. However, we observe that we can decouple the interdependence of the electrical conductivity and the Seebeck coefficient, and both parameters can be enhanced simultaneously.

As charge transport in conducting polymers cannot easily be described by the free-electron approximation used in crystalline semiconductors and metals, efforts to enhance our understanding and provide insight into the charge carrier characteristics of conducting polymers have led to the formulation of various polymer charge transport models.[47,56−59] For example, the proposed polymer charge transport model introduced by Kang and Snyder provides a relationship between the Seebeck coefficient and electrical conductivity. Here, the electrical conductivity is characterized by the transport function $\sigma_E(E)$ which for conducting polymers takes the form

$$\sigma_E(E, T) = \sigma_{E_0}(T)\left(\frac{E - E_t}{k_B T}\right)^s \quad (E > E_t) \tag{3}$$

The transport edge E_t and transport parameter s provide insight into the transport mechanism. E_t defines the energy below which no charge carriers contribute to the electrical conductivity. Thus, charge carriers must be thermally excited to contribute to the electrical conductivity. s provides a shape parameter for charge contribution relative to E_t. The position of the chemical potential with respect to E_t determines the relationship between S and σ, where the reduced chemical potential (η) is defined as

$$\eta = \frac{E_F - E_t}{k_B T} \tag{4}$$

Depending on η, σ and S can be modeled according to

$$S = \frac{k_B}{e}\left[s + 1 - \ln\left(\frac{\sigma}{\sigma_{E_0} s\Gamma(s)}\right)\right] \quad \eta \ll -1 \tag{5}$$

$$S = \frac{s k_B \pi^2}{3e}\left(\frac{\sigma}{\sigma_{E_0}}\right)^{-1/s} \quad \eta \gg 1 \tag{6}$$

Given that the energy-dependent scattering via the shape parameter s, doping via the reduced chemical potential, and the energy-independent transport parameter σ_{E_0} can be treated independently following the Kang–Snyder charge transport model, the combination of eqs 5 and 6 relative to the conductivity allows for the electrical transport to be characterized in terms of the calculated activation energy σ_{E_0}. Hence, the higher σ_{E_0} is the higher the potential ZT of the conducting polymer.[47] To determine σ_{E_0}, a profile of extrinsic dopants is used to correlate the relationship between S and σ. This has been done extensively for PEDOT and other polymers to determine both the transport parameter and σ_{E_0}. To compare differences between our PEDOT films, we fit the individual σ and S parameters to obtain the σ_{E_0} as a function of polymerization methods and counterion dopants. This analysis relies on the assumption that all characterizations of PEDOT until now using extrinsic doping are consistent, allowing us to fit a single data point to determine σ_{E_0}. Here, we demonstrate using the expected transport parameter $s = 1$ that the Seebeck coefficient and electrical conductivity relationship for our PEDOT samples increases σ_{E_0} in a similar trend to what is observed in comparing the respective power factors for these thin films (Figure 8C). This may also suggest that energy-dependent scattering is not being perturbed in our PEDOT thin films. This shows that σ_{E_0} is highly sensitive to the polymerization protocol and counterion dopant use in the fabrication of PEDOT thin films. An σ_{E_0} of 0.402 S cm^{-1} is obtained for PEDOT:Cl thin films prepared by using the CP method. The σ_{E_0} can be further increased to 12.2 S cm^{-1} when PEDOT:Cl thin films are prepared by following the VVPP method. Likewise, the σ_{E_0} can be increased from 48.5 to 235 S

https://doi.org/10.1021/acsapm.1c00069
ACS Appl. Polym. Mater. 2021, 3, 2938−2949

cm^{-1} when PEDOT:Tos thin films are prepared via the VVPP method instead of the CP method. From the standpoint of an undoped and highly disordered polymer with a transport parameter of $s = 3$, the σ_{E_0} is typically very small in the orders of $\leq$0.003 S cm^{-1}. This small σ_{E_0} is often related to polymers having poor thermoelectric properties that yield ZT values of $\leq$0.01 at 300 K.[47] Our results are particularly significant given that we can modulate the electronic structure of PEDOT thin films so that we obtain highly conducting and well-ordered polymers with unprecedented high σ_{E_0} values that are often found in acoustic phonon scattering dominated inorganic semiconductors with a transport parameter of $s = 1$.[60] This is encouraging given that a high σ_{E_0} value of 235 S cm^{-1} as calculated for VVPP PEDOT:Tos thin films, for example, can be contextualized by assuming a lattice thermal conductivity of 0.40 W m^{-1} K^{-1}, which has been reported for PEDOT:Tos with similar Seebeck and conductivity values,[15] will yield ZT values above 0.35 at 300 K. The role electrical conductivity plays in thermoelectric conductivity coupled with the enhancement of σ_{E_0} through intrinsic doping methodologies suggests that not only are higher ZT's attainable in conducting polymers but that further insight into the role of thermal conductivity as σ_{E_0} increases will be of significant interest in future studies.

CONCLUSION

This report demonstrates the effects that counterion dopant selection and polymerization protocols have on the structural doping and morphology of conducting polymer thin films. We found that crystallinity and crystallite orientation of PEDOT thin films can be enhanced when samples are fabricated following a VVPP synthesis approach. Our findings reveal that well-defined and highly conducting PEDOT thin films can be fabricated following the VVPP synthesis approach. Given the well-controlled morphology attained for PEDOT thin films by using the VVPP synthesis approach, we can then understand how the electronic structure of PEDOT is affected upon varying its oxidation levels due to the incorporation of different counterion dopants. This fundamental insight into the electronic structure of PEDOT was obtained by investigating any changes to its thermoelectric properties as a function of polymerization protocols and counterion dopants. We conclude that the narrow crystallite orientational distribution induced by the VVPP approach as well as the addition of the Tos^- counterion in PEDOT promotes the formation of thin films with enhanced thermoelectric properties (i.e., higher electrical conductivities, Seebeck coefficients, and power factors). Excitingly, we demonstrate that it is possible to tune the electronic structure of PEDOT so that the transport parameter is changed from $s = 3$ which is indicative of crystalline solids having a high level of impurities and scattering centers (e.g., ordered domains separated by regions with a large degree of disorder) to $s = 1$ which suggests the formation of crystalline solids with highly ordered domains that exhibit more of a bandlike electronic structure due effective supramolecular orbital mixing. The tunability of the transport parameter from $s = 3$ to $s = 1$ and the observation of an extremely high transport function are well sought after ingredients for obtaining thermoelectric materials with ZT values >0.1 at room temperature. Moreover, on the basis of our results, we believe it is realistic to achieve ZT values of >0.5 for PEDOT thin films fabricated following the VVPP synthesis approach and that comprise a Tos^- counterion dopant. Our results show the potential of highly conducting PEDOT:OTf films and the replacement with hydrogenosulfate counterions as an exciting avenue for future works. The investigation of hydrogenosulfate counterions that can be intrinsically coordinated during the polymerization process would show great promise as a counterion platform and further investigation into how enhancements from intrinsic parametrization differ from extrinsic material treatments, namely, with respect to the calculated σ_{E_0}.

We anticipate our findings will serve as a foundation in the development of well-defined and highly conducting polymer thin films beyond PEDOT that can serve as practical conduits for flexible sensors and power generators for wearable electronics. As empirical evidence has clearly shown that charge transport does not follow a single mechanism and recent work has demonstrated that the different modes of carrier transport may limit the maximum electrical characteristics obtainable for a given organic semiconductor, we encourage future research directions to focus on the development of mechanistic charge transport models that better account for changes in morphology, oxidation levels, and scattering impurities in polymer thin films.

ASSOCIATED CONTENT

Supporting Information

The Supporting Information is available free of charge at https://pubs.acs.org/doi/10.1021/acsapm.1c00069.

AFM images, XPS survey scans, and XPS data fits for S 2p and Cl 2p (PDF)

AUTHOR INFORMATION

Corresponding Author

Luisa Whittaker-Brooks − *Department of Chemistry, University of Utah, Salt Lake City, Utah 84112, United States*; orcid.org/0000-0002-1130-1306; Email: luisa.whittaker@utah.edu

Authors

Jonathan Ogle − *Department of Chemistry, University of Utah, Salt Lake City, Utah 84112, United States*

Daniel Powell − *Department of Chemistry, University of Utah, Salt Lake City, Utah 84112, United States*

Detlef-M. Smilgies − *Cornell High Energy Synchrotron Source, Cornell University, Ithaca, New York 14853, United States*; orcid.org/0000-0001-9351-581X

Dennis Nordlund − *Stanford Synchrotron Radiation Lightsource, SLAC National Accelerator Laboratory, Menlo Park, California 94025, United States*

Complete contact information is available at: https://pubs.acs.org/10.1021/acsapm.1c00069

Notes

The authors declare no competing financial interest.

ACKNOWLEDGMENTS

This work was supported by the NSF under award # DMR 1824263. Raman and XPS studies were supported by the NSF under award # CBET 2016191. GIWAXS studies were performed under NSF award # CBET 2018413 (University of Utah) and DMR 1332208 (Cornell High Energy Synchrotron Source). Use of the Stanford Synchrotron

Radiation Lightsource (SSRL), SLAC National Accelerator Laboratory, is supported by DOE, Office of Basic Energy Sciences under Contract number DE-AC02-76SF00515. LWB would also like to acknowledge the financial support from the Research Corporation for Science Advancement (USA) through a Cottrell Scholar Award and The Alfred P. Sloan Foundation (USA). We would like to thank Dr. Luis R. de Jesús for helpful discussions on the NEXAFS analysis.

REFERENCES

(1) Chiang, C. K.; Park, Y. W.; Heeger, A. J.; Shirakawa, H.; Louis, E. J.; MacDiarmid, A. G. Conducting Polymers: Halogen Doped Polyacetylene. *J. Chem. Phys.* **1978**, *69*, 5098−5104.
(2) Chiang, C. K.; Fincher, C. R.; Park, Y. W.; Heeger, A. J.; Shirakawa, H.; Louis, E. J.; Gau, S. C.; MacDiarmid, A. G. Electrical Conductivity in Doped Polyacetylene. *Phys. Rev. Lett.* **1977**, *39*, 1098−1101.
(3) MacDiarmid, A. G.; Mammone, R. J.; Kaner, R. B.; Porter, L.; Pethig, R.; Heeger, A. J.; Rosseinsky, D. R.; Gillespie, R. J.; Day, P. The Concept of 'Doping' of Conducting Polymers: The Role of Reduction Potentials. *Philos. Trans. R. Soc. London, Ser. A: Math. Phys. Sci.* **1985**, *314*, 3−15.
(4) Cao, Y.; Smith, P.; Heeger, A. J. Counter-ion Induced Processibility of Conducting Polyaniline and of Conducting Polyblends of Polyaniline in Bulk Polymers. *Synth. Met.* **1992**, *48*, 91−97.
(5) Epstein, A. J.; Ginder, J. M.; Zuo, F.; Woo, H. S.; Tanner, D. B.; Richter, A. F.; Angelopoulos, M.; Huang, W. S.; MacDiarmid, A. G. Insulator-to-Metal Transition in Polyaniline: Effect of Protonation in Emeraldine. *Synth. Met.* **1987**, *21*, 63−70.
(6) Sezen-Edmonds, M.; Loo, Y.-L. Beyond Doping and Charge Balancing: How Polymer Acid Templates Impact the Properties of Conducting Polymer Complexes. *J. Phys. Chem. Lett.* **2017**, *8*, 4530−4539.
(7) Vijayakumar, V.; Zhong, Y.; Untilova, V.; Bahri, M.; Herrmann, L.; Biniek, L.; Leclerc, N.; Brinkmann, M. Bringing Conducting Polymers to High Order: Toward Conductivities beyond 105 S cm^{-1} and Thermoelectric Power Factors of 2 mW m^{-1} K^{-2}. *Adv. Energy Mater.* **2019**, *9*, 1900266.
(8) Khan, Z. U.; Bubnova, O.; Jafari, M. J.; Brooke, R.; Liu, X.; Gabrielsson, R.; Ederth, T.; Evans, D. R.; Andreasen, J. W.; Fahlman, M.; Crispin, X. Acido-Basic Control of the Thermoelectric Properties of Poly(3,4-ethylenedioxythiophene)tosylate (PEDOT-Tos) Thin Films. *J. Mater. Chem. C* **2015**, *3*, 10616−10623.
(9) Wang, H.; Ail, U.; Gabrielsson, R.; Berggren, M.; Crispin, X. Ionic Seebeck Effect in Conducting Polymers. *Adv. Energy Mater.* **2015**, *5*, 1500044.
(10) Bubnova, O.; Khan, Z. U.; Wang, H.; Braun, S.; Evans, D. R.; Fabretto, M.; Hojati-Talemi, P.; Dagnelund, D.; Arlin, J.-B.; Geerts, Y. H.; Desbief, S.; Breiby, D. W.; Andreasen, J. W.; Lazzaroni, R.; Chen, W. M.; Zozoulenko, I.; Fahlman, M.; Murphy, P. J.; Berggren, M.; Crispin, X. Semi-Metallic Polymers. *Nat. Mater.* **2014**, *13*, 190−194.
(11) Rivnay, J.; Inal, S.; Collins, B. A.; Sessolo, M.; Stavrinidou, E.; Strakosas, X.; Tassone, C.; Delongchamp, D. M.; Malliaras, G. G. Structural Control of Mixed Ionic and Electronic Transport in Conducting Polymers. *Nat. Commun.* **2016**, *7*, 11287.
(12) Culebras, M.; Gómez, C. M.; Cantarero, A. Enhanced Thermoelectric Performance of PEDOT with Different Counter-Ions Optimized by Chemical Reduction. *J. Mater. Chem. A* **2014**, *2*, 10109−10115.
(13) King, Z. A.; Shaw, C. M.; Spanninga, S. A.; Martin, D. C. Structural, Chemical and Electrochemical Characterization of Poly-(3,4-Ethylenedioxythiophene) (PEDOT) Prepared with Various Counter-Ions and Heat Treatments. *Polymer* **2011**, *52* (5), 1302−1308.
(14) Hofmann, A. I.; Katsigiannopoulos, D.; Mumtaz, M.; Petsagkourakis, I.; Pecastaings, G.; Fleury, G.; Schatz, C.; Pavlopoulou, E.; Brochon, C.; Hadziioannou, G.; Cloutet, E. How To Choose Polyelectrolytes for Aqueous Dispersions of Conducting PEDOT Complexes. *Macromolecules* **2017**, *50*, 1959−1969.
(15) Bubnova, O.; Khan, Z. U.; Malti, A.; Braun, S.; Fahlman, M.; Berggren, M.; Crispin, X. Optimization of the Thermoelectric Figure of Merit in the Conducting Polymer Poly(3,4-ethylenedioxythiophene). *Nat. Mater.* **2011**, *10*, 429−33.
(16) Evans, D.; Fabretto, M.; Mueller, M.; Zuber, K.; Short, R.; Murphy, P. Structure-Directed Growth of High Conductivity PEDOT from Liquid-Like Oxidant Layers During Vacuum Vapor Phase Polymerization. *J. Mater. Chem.* **2012**, *22*, 14889−14895.
(17) Gueye, M. N.; Carella, A.; Faure-Vincent, J.; Demadrille, R.; Simonato, J.-P. Progress in Understanding Structure and Transport Properties of PEDOT-Based Materials: A Critical Review. *Prog. Mater. Sci.* **2020**, *108*, 100616.
(18) Gangopadhyay, R.; Das, B.; Molla, M. R. How does PEDOT Combine with PSS? Insights from Structural Studies. *RSC Adv.* **2014**, *4*, 43912−43920.
(19) Muñoz, W. A.; Singh, S. K.; Franco-Gonzalez, J. F.; Linares, M.; Crispin, X.; Zozoulenko, I. V. Insulator to Semimetallic Transition in Conducting Polymers. *Phys. Rev. B: Condens. Matter Mater. Phys.* **2016**, *94*, 205202.
(20) Xia, Y.; Sun, K.; Ouyang, J. Solution-Processed Metallic Conducting Polymer Films as Transparent Electrode of Optoelectronic Devices. *Adv. Mater.* **2012**, *24*, 2436−2440.
(21) Fabretto, M. V.; Evans, D. R.; Mueller, M.; Zuber, K.; Hojati-Talemi, P.; Short, R. D.; Wallace, G. G.; Murphy, P. J. Polymeric Material with Metal-Like Conductivity for Next Generation Organic Electronic Devices. *Chem. Mater.* **2012**, *24*, 3998−4003.
(22) Gueye, M. N.; Carella, A.; Massonnet, N.; Yvenou, E.; Brenet, S.; Faure-Vincent, J.; Pouget, S.; Rieutord, F.; Okuno, H.; Benayad, A.; Demadrille, R.; Simonato, J.-P. Structure and Dopant Engineering in PEDOT Thin Films: Practical Tools for a Dramatic Conductivity Enhancement. *Chem. Mater.* **2016**, *28*, 3462−3468.
(23) Rivnay, J.; Leleux, P.; Ferro, M.; Sessolo, M.; Williamson, A.; Koutsouras, D. A.; Khodagholy, D.; Ramuz, M.; Strakosas, X.; Owens, R. M.; Benar, C.; Badier, J. M.; Bernard, C.; Malliaras, G. G. High-Performance Transistors for Bioelectronics through Tuning of Channel Thickness. *Sci. Adv.* **2015**, *1*, No. e1400251.
(24) Jonsson, A.; Song, Z.; Nilsson, D.; Meyerson, B. A.; Simon, D. T.; Linderoth, B.; Berggren, M. Therapy using Implanted Organic Bioelectronics. *Sci. Adv.* **2015**, *1*, No. e1500039.
(25) Li, G.; Zhu, R.; Yang, Y. Polymer Solar Cells. *Nat. Photonics* **2012**, *6*, 153−161.
(26) Malti, A.; Edberg, J.; Granberg, H.; Khan, Z. U.; Andreasen, J. W.; Liu, X.; Zhao, D.; Zhang, H.; Yao, Y.; Brill, J. W.; Engquist, I.; Fahlman, M.; Wågberg, L.; Crispin, X.; Berggren, M. An Organic Mixed Ion-Electron Conductor for Power Electronics. *Adv. Sci.* **2016**, *3*, 1500305.
(27) Petsagkourakis, I.; Kim, N.; Tybrandt, K.; Zozoulenko, I.; Crispin, X. Poly(3,4-ethylenedioxythiophene): Chemical Synthesis, Transport Properties, and Thermoelectric Devices. *Adv. Electron. Mater.* **2019**, *5*, 1800918.
(28) Kim, G. H.; Shao, L.; Zhang, K.; Pipe, K. P. Engineered Doping of Organic Semiconductors for Enhanced Thermoelectric Efficiency. *Nat. Mater.* **2013**, *12*, 719−723.
(29) Park, T.; Park, C.; Kim, B.; Shin, H.; Kim, E. Flexible PEDOT electrodes with Large Thermoelectric Power Factors to Generate Electricity by the Touch of Fingertips. *Energy Environ. Sci.* **2013**, *6*, 788−792.
(30) Kyaw, A. K. K.; Yemata, T. A.; Wang, X.; Lim, S. L.; Chin, W. S.; Hippalgaonkar, K.; Xu, J. Enhanced Thermoelectric Performance of PEDOT:PSS Films by Sequential Post-Treatment with Formamide. *Macromol. Mater. Eng.* **2018**, *303*, 1700429.
(31) Wang, X.; Kyaw, A. K. K.; Yin, C.; Wang, F.; Zhu, Q.; Tang, T.; Yee, P. I.; Xu, J. Enhancement of Thermoelectric Performance of PEDOT:PSS Films by Post-Treatment with a Superacid. *RSC Adv.* **2018**, *8*, 18334−18340.
(32) Lee, Y.-Y.; Choi, G. M.; Lim, S.-M.; Cho, J.-Y.; Choi, I.-S.; Nam, K. T.; Joo, Y.-C. Growth Mechanism of Strain-Dependent

Morphological Change in PEDOT:PSS Films. *Sci. Rep.* **2016**, *6*, 25332.
(33) Chen, G.; Rastak, R.; Wang, Y.; Yan, H.; Feig, V.; Liu, Y.; Jiang, Y.; Chen, S.; Lian, F.; Molina-Lopez, F.; Jin, L.; Cui, K.; Chung, J. W.; Pop, E.; Linder, C.; Bao, Z. Strain- and Strain-Rate-Invariant Conductance in a Stretchable and Compressible 3D Conducting Polymer Foam. *Matter* **2019**, *1*, 205−218.
(34) Jiang, Z. GIXSGUI: a MATLAB Toolbox for Grazing-Incidence X-ray Scattering Data Visualization and Reduction, and Indexing of Buried Three-Dimensional Periodic Nanostructured Films. *J. Appl. Crystallogr.* **2015**, *48*, 917−926.
(35) Ogle, J.; Powell, D.; Amerling, E.; Smilgies, D.-M.; Whittaker-Brooks, L. Quantifying Multiple Crystallite Orientations and Crystal Heterogeneities in Complex Thin Film Materials. *CrystEngComm* **2019**, *21*, 5707−5720.
(36) Ouyang, J.; Xu, Q.; Chu, C.-W.; Yang, Y.; Li, G.; Shinar, J. On the Mechanism of Conductivity Enhancement in Poly(3,4-ethylenedioxythiophene):poly(styrene sulfonate) Film through Solvent Treatment. *Polymer* **2004**, *45*, 8443−8450.
(37) Łapkowski, M.; Proń, A. Electrochemical Oxidation of Poly(3,4-ethylenedioxythiophene) — "in situ" Conductivity and Spectroscopic Investigations. *Synth. Met.* **2000**, *110*, 79−83.
(38) Chen, S.; Petsagkourakis, I.; Spampinato, N.; Kuang, C.; Liu, X.; Brooke, R.; Kang, E. S. H.; Fahlman, M.; Crispin, X.; Pavlopoulou, E.; Jonsson, M. P. Unraveling Vertical Inhomogeneity in Vapour Phase Polymerized PEDOT:Tos Films. *J. Mater. Chem. A* **2020**, *8*, 18726−18734.
(39) Wang, X.; Zhang, X.; Sun, L.; Lee, D.; Lee, S.; Wang, M.; Zhao, J.; Shao-Horn, Y.; Dincă, M.; Palacios, T.; Gleason, K. K. High Electrical Conductivity and Carrier Mobility in oCVD PEDOT Thin Films by Engineered Crystallization and Acid Treatment. *Sci. Adv.* **2018**, *4*, No. eaat5780.
(40) Shi, W.; Yao, Q.; Qu, S.; Chen, H.; Zhang, T.; Chen, L. Micron-Thick Highly Conductive PEDOT Films Synthesized via Self-Inhibited Polymerization: Roles of Anions. *NPG Asia Mater.* **2017**, *9*, No. e405.
(41) Xing, K. Z.; Fahlman, M.; Chen, X. W.; Inganäs, O.; Salaneck, W. R. The Electronic Structure of Poly(3,4-ethylene-dioxythiophene): Studied by XPS and UPS. *Synth. Met.* **1997**, *89*, 161−165.
(42) Petsagkourakis, I.; Pavlopoulou, E.; Portale, G.; Kuropatwa, B. A.; Dilhaire, S.; Fleury, G.; Hadziioannou, G. Structurally-driven Enhancement of Thermoelectric Properties within Poly(3,4-ethylenedioxythiophene) thin Films. *Sci. Rep.* **2016**, *6* (1), 30501.
(43) Muñoz, W. A.; Crispin, X.; Fahlman, M.; Zozoulenko, I. V. Understanding the Impact of Film Disorder and Local Surface Potential in Ultraviolet Photoelectron Spectroscopy of PEDOT. *Macromol. Rapid Commun.* **2018**, *39* (4), 1700533.
(44) Crispin, X.; Jakobsson, F. L. E.; Crispin, A.; Grim, P. C. M.; Andersson, P.; Volodin, A.; van Haesendonck, C.; Van der Auweraer, M.; Salaneck, W. R.; Berggren, M. The Origin of the High Conductivity of Poly(3,4-ethylenedioxythiophene)-Poly-(styrenesulfonate) (PEDOT-PSS) Plastic Electrodes. *Chem. Mater.* **2006**, *18*, 4354−4360.
(45) Hiszpanski, A. M.; Loo, Y.-L. Directing the Film Structure of Organic Semiconductors via Post-Deposition Processing for Transistor and Solar Cell Applications. *Energy Environ. Sci.* **2014**, *7*, 592−608.
(46) Kaiser, A. B. Electronic Transport Properties of Conducting Polymers and Carbon Nanotubes. *Rep. Prog. Phys.* **2001**, *64* (1), 1−50.
(47) Kang, S. D.; Snyder, G. J. Charge-Transport Model for Conducting Polymers. *Nat. Mater.* **2017**, *16*, 252−257.
(48) De Jesus, L. R.; Horrocks, G. A.; Liang, Y.; Parija, A.; Jaye, C.; Wangoh, L.; Wang, J.; Fischer, D. A.; Piper, L. F. J.; Prendergast, D.; Banerjee, S. Mapping Polaronic States and Lithiation Gradients in Individual V_2O_5 Nanowires. *Nat. Commun.* **2016**, *7* (1), 12022.
(49) Stöhr, J. *NEXAFS Spectroscopy*; Springer-Verlag: Berlin, 1992; Vol. *25*.
(50) Lee, V.; Whittaker, L.; Jaye, C.; Baroudi, K. M.; Fischer, D. A.; Banerjee, S. Large-Area Chemically Modified Graphene Films: Electrophoretic Deposition and Characterization by Soft X-ray Absorption Spectroscopy. *Chem. Mater.* **2009**, *21*, 3905−3916.
(51) Ogle, J.; Lahiri, N.; Jaye, C.; Tassone, C. J.; Fischer, D. A.; Louie, J.; Whittaker-Brooks, L. Semiconducting to Metallic Electronic Landscapes in Defects-Controlled 2D π-d Conjugated Coordination Polymer Thin Films. *Adv. Funct. Mater.* **2021**, *31*, 2006920.
(52) Watts, B.; Swaraj, S.; Nordlund, D.; Lüning, J.; Ade, H. Calibrated NEXAFS Spectra of Common Conjugated Polymers. *J. Chem. Phys.* **2011**, *134*, 024702.
(53) Schuettfort, T.; Thomsen, L.; McNeill, C. R. Observation of a Distinct Surface Molecular Orientation in Films of a High Mobility Conjugated Polymer. *J. Am. Chem. Soc.* **2013**, *135*, 1092−1101.
(54) Kumar, P.; Zaia, E. W.; Yildirim, E.; Repaka, D. V. M.; Yang, S. W.; Urban, J. J.; Hippalgaonkar, K. Polymer Morphology and Interfacial Charge Transfer Dominate over Energy-Dependent Scattering in Organic-Inorganic Thermoelectrics. *Nat. Commun.* **2018**, *9* (5347), 1−10.
(55) Jin Bae, E.; Hun Kang, Y.; Jang, K.-S.; Yun Cho, S. Enhancement of Thermoelectric Properties of PEDOT:PSS and Tellurium-PEDOT:PSS Hybrid Composites by Simple Chemical Treatment. *Sci. Rep.* **2016**, *6* (1), 18805.
(56) Russ, B.; Glaudell, A.; Urban, J. J.; Chabinyc, M. L.; Segalman, R. A. Organic Thermoelectric Materials for Energy Harvesting and Temperature Control. *Nat. Rev. Mater.* **2016**, *1* (10), 16050.
(57) Poehler, T. O.; Katz, H. E. Prospects for Polymer-based Thermoelectrics: State of the Art and Theoretical Analysis. *Energy Environ. Sci.* **2012**, *5*, 8110−8115.
(58) Hofacker, A. Critical Charge Transport Networks in Doped Organic Semiconductors. *Commun. Mater.* **2020**, *1*, 1−9.
(59) Liu, C.; Huang, K.; Park, W.-T.; Li, M.; Yang, T.; Liu, X.; Liang, L.; Minari, T.; Noh, Y.-Y. A Unified Understanding of Charge Transport in Organic Semiconductors: The Importance of Attenuated Delocalization for the Carriers. *Mater. Horiz.* **2017**, *4*, 608−618.
(60) Fistul, V. I. *Heavily Doped Semiconductors*; Springer: New York, 1969; Vol. *1*, Chapters 3 and 4.

https://doi.org/10.1021/acsapm.1c00069
ACS Appl. Polym. Mater. 2021, 3, 2938−2949